Amino-functionalized microporous hybrid silica membranes

G.G. Paradis[a]

R. Kreiter[a]

M.M.A. van Tuel[a]

A. Nijmeijer[b]

Jaap F. Vente[a]

[a]ECN, P.O. Box 1, 1755 ZG Petten, The Netherlands
[b]Inorganic Membranes, Department of Science and Technology and MESA + Institute for Nanotechnology, University of Twente

Published in J. Mater. Chem., 2012, 22, 7258–7264

ECN-W--12-009 MARCH 2012

Journal of Materials Chemistry

Dynamic Article Links

Cite this: J. Mater. Chem., 2012, 22, 7258

www.rsc.org/materials

PAPER

Amino-functionalized microporous hybrid silica membranes

Goulven G. Paradis,[a] Robert Kreiter,[a] Marc M. A. van Tuel,[a] Arian Nijmeijer[b] and Jaap F. Vente*[a]

Received 24th October 2011, Accepted 27th January 2012
DOI: 10.1039/c2jm15417j

The present study describes the effect of the incorporation of amino-functionalized terminating groups on the behaviour and performance of an organic–inorganic hybrid silica membrane. A primary amine, a mixed primary and secondary amine, and an imidazole functionality were selected. The molar ratio of the amino-functionalized precursors in the matrix forming 1,2-bis(triethoxysilyl)ethane (BTESE) precursor was varied in the range of 25–100 mol%. Strong water adsorption, which remains at temperatures up to 523 K, was found for all membranes. The observed low gas permeances and contrasting high water fluxes in pervaporation were explained in relation to the strong water adsorption. XPS measurements indicate a relation between the concentration of amino functional groups in the hybrid layers and the starting amine concentration of the sols. XPS measurements also revealed the existence of a maximum loading of the amino-functionalized precursor. Depending on the precursor, a maximum N/Si element ratio between 0.07 and 0.45 was found. At amine concentrations higher than a precursor dependent threshold value, membrane selectivity is constant over the range of amine concentrations. For alcohol/water (95/5 wt%) feed mixtures, the observed water concentrations in the permeate were over 90 wt% for EtOH and 95 wt% for *n*-BuOH dehydration.

Introduction

Molecular separations using inorganic microporous membranes (pores $\leq$ 2 nm) are governed by a combination of molecular sieving effects and membrane affinity. Key methods to direct the dominant separation mechanism are tuning the pore size and tailoring the affinity by the introduction of functional groups.[1] Until recently, microporous inorganic silica membranes were the subject of most of the research efforts in this field, and many of these studies focused on microstructure control.[2] Successful examples of highly selective gas separation and pervaporation membranes were reported.[2,3] Despite their relative ease of synthesis and a high thermal resistance, silica membranes have not become a commercial success. This is, most likely, related to their low hydrothermal stability.[4] This is especially apparent in separations in which water is present at high temperatures, such as water gas shift conditions, or high temperature dewatering of organic solvents.[5,6]

Recently, we developed hybrid organic–inorganic HybSi® membranes to overcome the stability boundaries of inorganic silica.[7] The introduction of an organic fragment in a silica network by using bridged bis-silane precursors leads to membranes having a life time of 1000 days in alcohol dehydration at high temperature without selectivity decrease.[8] The governing separation mechanism of this hybrid silica network is based on molecular sieving, as the dehydration performance depends on the alkyl bridge length.[9] The incorporation of well-defined functional groups has been studied in relation with ion transport.[10] For molecular separation applications, a limited number of attempts have been made to functionalize microporous silica membranes,[11] whereas this has not been reported for organic–inorganic hybrid silica membranes. The influence of the shape, length, and flexibility of the organic bridges in the hybrid silica network on the membrane pore size, structure, and affinity was recently described by Castricum *et al.*[12] Strong differences in gas permeance properties and pervaporation performances were observed.

Here, we present the first results on the incorporation of functional terminating groups in microporous hybrid silica (HybSi®) membranes. The aim of the present study was to explore the further hydrophilization of organic–inorganic hybrid materials whilst keeping the organic fragments the backbone intact. Three different triethoxysilanes with an amine group were selected for this purpose and introduced in a matrix of 1,2-bis (triethoxysilyl)ethane (BTESE), assuming these would increase the affinity for CO_2 and for water. As a first candidate the primary amine 3-aminopropyltriethoxysilane (PA) was chosen. Further, an imidazole, *N*-(3-triethoxysilylpropyl)-4,5-dihydroimidazole (IM), and a long alkyl chain with a primary and a secondary amine group, 3-(2-aminoethylamino)propyltrimethoxysilane (LDA), were selected (Fig. 1).

The use of 3-aminopropyltriethoxysilane (PA) was reported by Brinker *et al.* in periodic mesoporous silica thin films by

[a]*ECN, P.O. Box 1, 1755 ZG Petten, The Netherlands. E-mail: vente@ecn.nl; Fax: +31 (0) 224 56 86 15; Tel: +31 (0) 224 56 49 16*
[b]*Inorganic Membranes, Department of Science and Technology and MESA + Institute for Nanotechnology, University of Twente, P.O. Box 217, 7500 AE Enschede, The Netherlands*

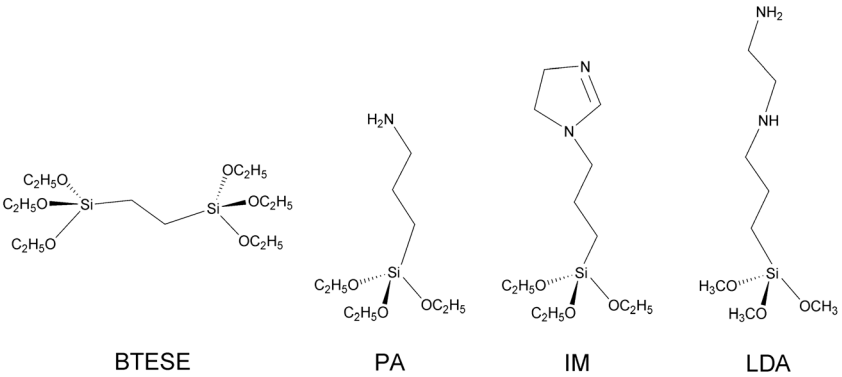

Fig. 1 Overview of the precursors.

co-condensation with tetraethoxysilane (TEOS) in a so-called EISA procedure.[13] Later it was used for surface functionalization of siliceous materials[14–18] or biocompatible materials.[19,20] Xomeritakis *et al.*[21] presented the first microporous PA-functionalized silica membranes for CO_2 separation, followed by a comparison with nickel doped silica membranes.[22] The two other precursors are novel precursors in membrane technology. The membrane properties were determined using gas permeation tests and alcohol dehydration measurements.

Experimental section

1,2-Bis(triethoxysilyl)ethane (BTESE, ABCR, 97%), 3-aminopropyltriethoxysilane (PA, ABCR, 98%), *N*-(3-triethoxy-silylpropyl)-4,5-dihydroimidazole (IM, ABCR, 97%), 3-(2-aminoethylamino)propyltrimethoxysilane (LDA, ABCR, 96%), nitric acid (69 wt%, Aldrich), and EtOH (p.a. Aldrich) were used as received. Water was deionized at 18 MΩ cm^{-1} using a Millipore purification system. The abbreviations used for the precursors refer to their structure. PA, IM, and LDA stand for Primary Amine, Imidazole, and Linear DiAmine.

Pure triethoxysilane sols were synthesized using a single-step synthesis. The desired amounts of nitric acid, distilled water and EtOH were premixed. Amino-functionalized precursors were subsequently added in one shot to the nitric acid, distilled water and EtOH mixture and the sols were refluxed for three hours under stirring at 333 K. The sols based on two precursors were prepared in a two-step procedure. Nitric acid, distilled water and EtOH were premixed in this order and BTESE was subsequently added. This mixture was heated at 333 K for 3 hours under stirring. The amino-functionalized precursor was diluted in EtOH and added to the BTESE sol. This final mixture was stirred at RT for 30 min before coating. Precursor amounts were adjusted to obtain final molar concentrations of 25, 50, and 75 mol% of the amino-functionalized precursor.

The membrane layers were coated on 30 cm long tubular mesoporous γ-Al_2O_3 supports[23] in a class 1000 clean room. Sols were filtered over 0.8 μm cellulose acetate (CA) Whatman® filters before coating. The coating procedure and setup are described by Bonekamp *et al.*[23] The withdrawal speed of the dip coating procedure was set at 5 mm s^{-1}. After overnight drying in the clean room, the membranes were heat treated at 523 K under N_2 for two hours with heating and cooling rates of 0.5 °C min^{-1}. Four cycles of vacuum–N_2 purge of one hour each were performed before the heat treatment. All membranes were sealed using stainless steel caps and graphite as packing material.[24] One single membrane for each composition was used for both gas permeation and all pervaporation measurements. Reproducibility was checked on selected membranes such as PA25.

Colloid sizes of the sols were determined by dynamic light scattering (DLS) using a Malvern Zetasizer nano ZS. All sols were measured at the same silica concentration of 0.5 mol L^{-1}.

Layer thickness determinations and surface characterizations were carried out on a high resolution JEOL JSM-6330F Field Emission Scanning Electron Microscope (SEM). Circular samples were cut from the middle of the 30 cm heat-treated membrane, fractured, cleaned with compressed air and sputtered before measurement. These layer thicknesses were used to calculate the permeability of the membranes.

X-Ray Electron Spectroscopy (XPS) measurements were performed on heat treated membrane samples using a Quantera SXM (Scanning XPS Microprobe) from Physical Electronics. Spectra were acquired using an Al Kα radiation monochromatic at 1486.6 eV. Quoted binding energies are referred to the C1s emission at 283.65 eV from Si–C*–C carbon atom as the network backbone consists of Si–C–C–Si. The expected atomic N/Si ratios were calculated on the basis of a fully condensed network. Measurements were performed on the same sample as used for SEM measurements. Depth profile thicknesses were calculated from the sputtering time, assuming that the sputter-speed on the hybrid silica membrane surface is equivalent to the speed on a SiO_2 network.

Permporometry of supported hybrid membranes was carried out with water vapour as the condensable gas and He as the permeating gas.[25] A drying temperature of 473 K and a measurement temperature of 314 K were used. Pore size distributions were determined using the Kelvin equation.

Single gas permeance measurements were performed at 523, 423 and 323 K with feed pressures from 9 to 3 bara. Pressure differences of 2 bara were applied except for the point at 3 bara feed pressure for which a pressure difference of 1.5 bara was used. A retentate flow of 50 mL min^{-1} was applied for all measurements. Measurements were performed using He, H_2, N_2, CH_4, and CO_2 in a 5.0 purity. Before measurement, each membrane was dried for two hours at 523 K under N_2. H_2 permeance measurements were performed as first and last measurement.

Pervaporation measurements were carried out with feed mixtures of alcohol/water (95/5 wt%) at 368 K and 343 K for *n*-BuOH and EtOH respectively. Permeate pressure was kept constant at 10 mbar and measurements were performed at regular intervals. More details on the experimental set up can be found elsewhere.[8] Throughout this paper, the membranes and sols are named according to the precursor used and the molar concentration of this precursor in the sol. For example, the PA/BTESE sols and membranes with 25, 50, and 75 mol% of PA are named PA25, PA50, and PA75 respectively. A sample based on PA only is named PA100.

Results

The development of a sol suitable for the formation of a microporous top layer involves the use of an acid-catalyst rather than a basic one.[26] The incorporation of amine groups may thus lead to complications due to their basic nature and possible catalytically activity. Indeed, in the case of PA-based sols, instantaneous precipitation was observed when the acid/water mixture was added to the BTESE/PA-based mixture. To counter this, amine-protection by protonation with HCl was attempted.[13,21] The obtained BTESE/PA sols were clear and homogeneous, but during drying phase separation into an opaque top fraction and a clear bottom fraction was observed. The use of a two-step synthesis by addition of non-hydrolyzed PA precursor to a pre-hydrolyzed BTESE sol was tried as the second possible alternative.[18,21] A BTESE sol was synthesized with compositional ratios of $Si/EtOH/H^+/H_2O = 1/11.4/0.12/6$. Subsequently, a PA solution in ethanol of the same silicon concentration of 1.5 M was added to the BTESE sol. After heating this mixture to 333 K gelation occurred within a few minutes. After reducing the silicon concentrations to 0.5 M for both the BTESE sol and the PA solution and setting the reaction temperature for the second step at RT, amino-functionalized sols were obtained. These sols are stable in time at RT and have suitable particle sizes (5–10 nm) for coating of thin microporous layers. Based on these observations, the two step synthesis was selected for further study. The sol development was performed on PA/BTESE sols, after which the same procedure was adopted for IM/BTESE and LDA/BTESE sols.

Sols based on the sole amino-functionalized precursor were synthesized following a one-step synthesis procedure with ratios of $Si/EtOH/H^+/H_2O = 1/11.4/0.06/3$ at a silica concentration of 1.5 mol L^{-1}. Particles sizes of 2 to 3 nm were obtained for the pure PA sols. A possible explanation for these smaller particle sizes is the formation of small PA clusters through hydrogen bonding between primary amine groups,[27] inhibiting chain growth. After coating at a silica concentration of 0.3 mol L^{-1} on the γ-Al_2O_3 support and the subsequent heat treatment, SEM measurements showed thin and defect free amino-functionalized hybrid silica layers (Fig. 2). The thicknesses of PA-based membranes ranged from 80 to 180 nm and no infiltration into the support layer was observed. Membranes containing the precursors IM or LDA were also defect free with thicknesses between 100 and 300 nm.

Atomic N/Si ratios of membrane samples were determined using XPS measurements on a sputtered surface. The expected trend of an increase of the N/Si ratios as the concentration of amino-functionalized precursor increases was in all cases observed (Table 1). Compared to the expected N/Si ratios, the measured values were significantly lower. The smallest differences were observed for the LDA-based membranes. In addition, measurements were performed on green and heat treated powders for PA75. Measured N/Si ratios were 0.62 for the green and 0.52 for the heat treated powder. In contrast to the membrane samples, these values are in good accordance with the expected values.

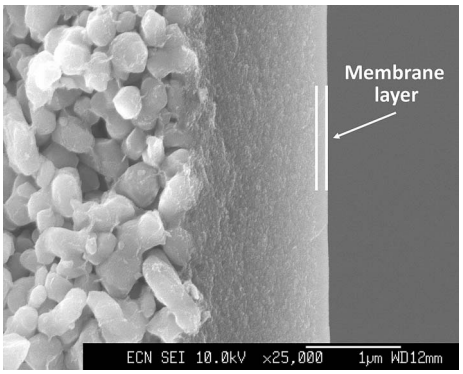

Fig. 2 SEM image of a cross-section of an PA50 membrane.

Fig. 3 shows the XPS depth profile analysis on the PA75 heat-treated membrane. Four sections could be distinguished: a first layer of about 15 nm rich in adventitious carbon (A), the effective hybrid layer of about 65 nm (B), about 60 nm of infiltrated sol in the γ-Al_2O_3 support (C), and the clean γ-Al_2O_3 support (D). The residual C, Si, and N measured at depths of over 140 nm are resulting from element pushing by the sputtering beam. The actual membrane layer (B) had a N/Si ratio of about 0.08 in agreement with the value measured on the sputtered surface of the same sample.

The PA membranes do not show any dependence on the average pressure in gas permeance measurements. Such a pressure dependency of the permeance would be an indication for viscous flow through defects. In accordance with permporometry (Fig. 4), the absence of viscous flow is therefore taken as an indication of the membrane quality and the absence of large defects.[28] In all cases minor (<10%) differences between the first and the second H_2 permeance measurement were observed, so no major structural changes occurred over the measurement series.

More importantly, the amount of PA in the BTESE matrix has a strong influence on the H_2 permeability. A nearly linear decrease of an order of magnitude was observed for the H_2 permeability with increasing PA molar concentration at constant

Table 1 Measured (*M*) and expected (*E*) N/Si ratios of heat treated amino-functionalized membranes

Mol% of amino-precursor	PA		IM		LDA	
	M	*E*	*M*	*E*	*M*	*E*
25%	0.04	0.14	0.016	0.28	0.14	0.28
50%	0.06	0.33	0.06	0.66	0.32	0.66
75%	0.07	0.63	0.15	1.25	0.45	1.25
100%	0.3	1	0.62	2	0.52	2

Table 2 H_2/N_2 and CO_2/N_2 permeability ratios of BTESE and BTESE/PA membranes at various temperatures

	H_2/N_2			CO_2/N_2		
Membrane	323 K	423 K	523 K	323 K	423 K	523 K
BTESE	15.2	14.5	13.6	10.0	4.9	3.2
PA25	9.0	10.3	11.8	8.3	4.9	3.2
PA50	13.7	15.1	16.9	9.1	5.8	3.6
PA75	12.1	18.8	20.7	4.0	4.9	2.9
PA100	4.3	7.2	13.9	1.2	1.5	1.8

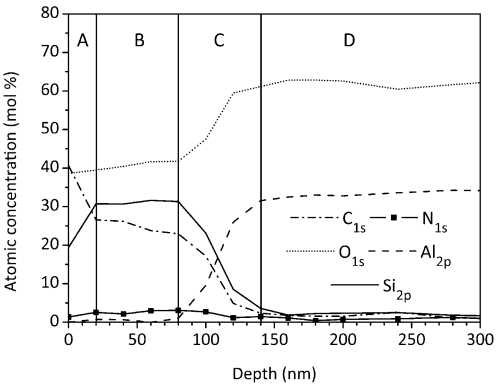

Fig. 3 Depth profile of the PA75 supported layer. A: surface rich in C due to adventitious carbon deposition; B: effective hybrid layer; C: layer infiltrated in the γ-Al_2O_3 support; and D: γ-Al_2O_3 support.

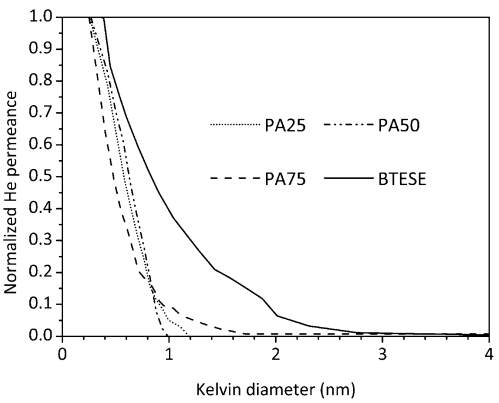

Fig. 4 Normalized pore size distributions of the BTESE/PA membranes and a BTESE membrane.

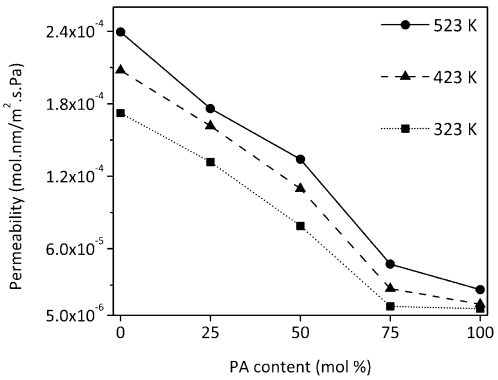

Fig. 5 H_2 permeability as a function of concentration of PA in the BTESE matrix at 323, 423, and 523 K.

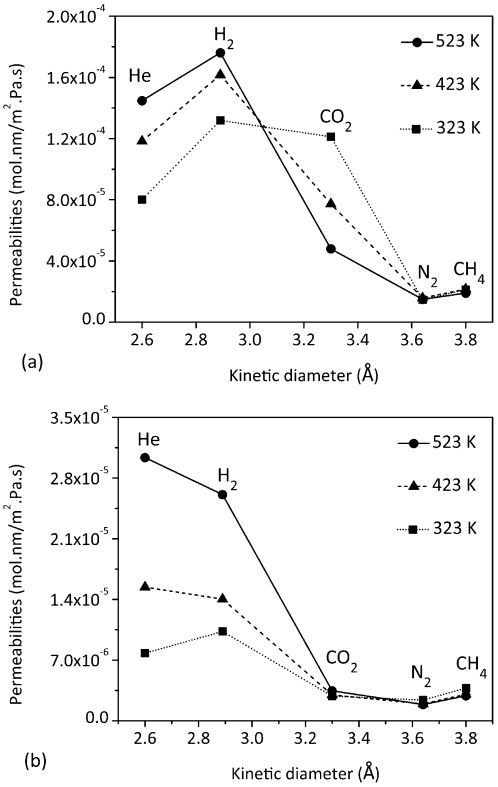

Fig. 6 Permeability of PA25 (a) and PA100 (b) against the kinetic diameter of the gas at different measurement temperatures.

temperature (Fig. 5, as for all figures the lines connecting the data points are here to only guide the reader and are not a fitting) with very low values of about 1×10^{-5} mol nm per m^2 s Pa for PA75 and PA100. This trend was observed over a 200 K temperature range.

The permeabilities are plotted against the kinetic diameter for all measured gases at different temperatures in Fig. 6. For PA25 only minor H_2 and He permeability changes with temperature were observed, whereas for PA100 a major permeability increase was observed for these gases. In contrast, for PA25 the CO_2 permeability is significantly higher at the lowest measurement temperature of 323 K, whereas no temperature dependency of the CO_2 permeability was observed for PA100. The N_2 and CH_4 permeabilities were constant at all temperatures for both membranes. All membranes exhibited H_2/N_2 permeability ratios higher than the Knudsen value of 3.74 (Table 2).[29] This ratio is relatively constant at the measured temperatures for BTESE. However, the measurement temperature clearly affects the H_2/N_2 permeability ratio for the PA membrane series. At the lowest measurement temperature of 323 K, the BTESE membrane exhibited the highest ratio of 15.2 and the lowest ratios were found for PA25 and PA100. However at 523 K, all membranes showed ratios higher than 10 and even higher than 20 for PA75. Surprisingly, PA100 showed an equivalent ratio to BTESE at

523 K, despite its low performance at 323 K. In contrast, all PA membranes show higher H_2/N_2 permeability ratio at higher temperatures. This effect seems to be stronger for higher concentrations of PA in the membrane. For PA100 the strongest relative increase of the H_2/N_2 permeability ratio was observed, ranging from 4.3 at 323 K to almost 13.9 at 523 K. This represents an increase of 220%. This increase in ratio results from a higher H_2 permeability combined to a constant N_2 permeability.

The CO_2/N_2 permeability ratio was also affected by the temperature and the PA content. BTESE, PA25 and PA50 exhibited similar values at 323 K, while for PA75 and PA100 lower ratios were found at the same temperature. At the two higher measurement temperatures the CO_2/N_2 ratio drops for all membranes except the PA100. For this membrane type the CO_2/N_2 ratio increased slightly with temperature.

Membrane performance in single gas permeance experiments clearly depends on the PA concentration in the BTESE matrix. In addition, the permporometry measurements indicate that water adsorbs strongly in the PA containing membranes. Therefore, we were interested if these effects would also translate to the water selectivity and transport through these membranes. To this end, all membranes were tested for dehydration of alcohol/water (95/5 wt%) mixtures by pervaporation. The PA membranes were first tested in the dehydration of EtOH/H_2O mixtures for several days. Subsequently, after drying at RT for two weeks, the membranes were used for dehydration of a *n*-BuOH/H_2O mixture, and finally again put in an EtOH/H_2O mixture without drying in between. The values presented are averaged over several days of testing.

In the first series of EtOH dehydration measurements all PA containing membranes exhibited water concentrations of 43–67 wt% in the permeate, compared to 90 wt% for a BTESE membrane (Fig. 7). The lowest water concentration was observed for PA25 to be 43 wt%, whereas the highest was for PA50 and PA75 with respectively 65 and 67 wt% of water in the permeate. In the separation of a *n*-BuOH/H_2O mixture all membranes exhibited water purities in the permeate of at least 93 wt%. Over the range of PA concentrations, a similar trend was observed as for the EtOH dehydration. All membranes had a high selectivity in this separation and PA50 and 75 were equivalent to the reference BTESE membrane. In the subsequent second dehydration test in the EtOH/H_2O mixture, all PA exhibited a higher water concentration in the permeate than in the first measurement series. Interestingly, the differences between membranes over the range of PA concentrations are still the same in this second set of measurements. Apparently, the influence of the measurement sequence on the membranes was the same for all PA/BTESE ratios.

The amount of amino-functionalized precursor in the membrane has a pronounced influence on the selectivity for water. Therefore, we aimed to also explore the influence of the nature of the amino substituent on the membrane behaviour. The precursors selected consist of a combination of a secondary and IM/BTESE and LDA/BTESE mixed membranes were tested first in a *n*-BuOH/H_2O mixture and subsequently in a EtOH/H_2O mixture without intermediate drying.

For IM/BTESE membranes in *n*-BuOH dehydration, the same trend was observed as for PA/BTESE (Fig. 8). All membranes, except the IM25, were highly selective for water. The selectivities of IM75 and IM100 are high and 95 and 92 wt% of water in the permeate were obtained respectively. In EtOH dehydration, a much lower selectivity was observed for IM25 giving only 40 wt % of water in the permeate. In this mixture, IM75 is slightly less selective than its 50 or 100 wt% counterpart.

For all LDA/BTESE membranes in *n*-BuOH dehydration the water purities in the permeate were comparable to a BTESE reference membrane and in the range of 96 to 98 wt% (Fig. 9). In EtOH dehydration the water concentration in the permeate ranged from 86 to 93 wt%. In this case no clear difference in selectivity was observed for any of the membranes compositions, in contrast to the other two precursors. Interestingly, the LDA75 and LDA100 membranes were highly selective for the separation of water from EtOH, having respectively 91 and 93 wt% of water in the permeate.

The water fluxes ranged from 1.6 to 6.2 kg m^{-2} h^{-1} in *n*-BuOH dehydration and from 0.2 to 3.4 in kg m^{-2} h^{-1} EtOH dehydration (Table 3). For all membranes the fluxes in EtOH dehydration were a factor two to four lower than in *n*-BuOH dehydration. Only the IM50 membrane exhibited both a relatively high flux and high selectivity in EtOH dehydration, with 92 wt% of water in the permeate and a water flux of 2.4 kg m^{-2} h^{-1}. As a comparison, a previously published BTESE membrane exhibited 90 wt% of water in the permeate at a water flux of 1.5 kg m^{-2} h^{-1}.[9]

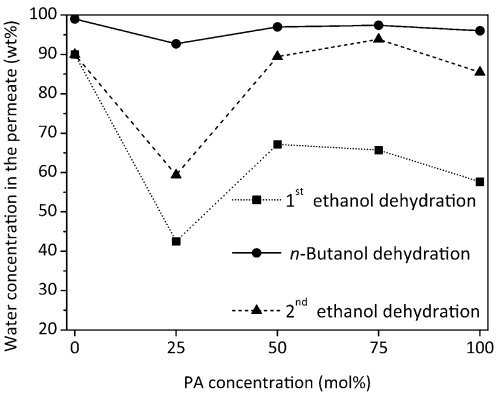

Fig. 7 Water concentration in the permeate for dehydration of EtOH and *n*-BuOH using BTESE/PA membranes.

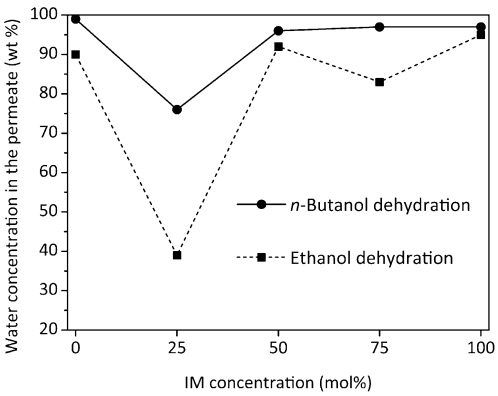

Fig. 8 Water concentration in the permeate in the dehydration of EtOH and *n*-BuOH for IM/BTESE membranes.

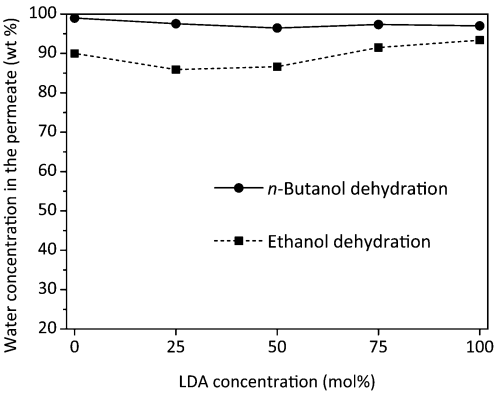

Fig. 9 Water concentration in the permeate in the dehydration of EtOH and *n*-BuOH for LDA/BTESE membranes.

Table 3 Water fluxes (kg m^{-2} h^{-1}) of the three types of membranes for the dehydration of alcohol/water (95/5 wt%) mixtures

Alcohol	PA J_{H_2O}	IM J_{H_2O}	LDA J_{H_2O}
n-BuOH	1.6–3.9	3.9–6.2	2.2–4.1
EtOH	0.2–2.1	1–3.4	0.35–1.1

Discussion

In this study, functionalized membranes containing three different amino functional precursors were successfully incorporated into a hybrid silica network over a wide range of molar ratios. The amino-functionalized precursors have a pronounced influence on the membrane properties, as is apparent from the gas permeance data and the performance in alcohol dehydration.

The thin hybrid layers proved to be free of macrodefects, as no indications of viscous flow were found during single gas permeation. In addition, XPS confirmed the amine functionalization of the BTESE network. However the measured N/Si ratios on heat-treated membranes were significantly lower than those expected. Still and as expected, the N/Si ratio does increase with increasing amount of PA in the sol. Hence, the membranes properties can be attributed to the presence of these amino-functionalized precursors as well as to their concentration in the BTESE network.

All measurements suggest that the polar nature of the amine in PA enhanced the water adsorption capacity of the membranes. Combined to a microporous structure, this resulted in unprecedented gas tight membranes that are at the same time water permeable.

The low permeability of the PA membranes and the decrease of the H_2 permeability with increasing PA concentration can be ascribed to progressive pore blocking by adsorbed water. The AP25 slightly deviates from the trend. Nevertheless, this progressive increase of the water affinity of these membranes resulted in a significant decrease of the CO_2 affinity, as indicated by the large decrease of the CO_2/N_2 ratios from BTESE to PA100 and the constant CO_2 permeance of PA100 over the temperature range. This is probably due to inhibition of the N_2 transport and to the shielding of the possible CO_2 adsorption sites (NH_2 and/or OH) by adsorbed water. For CO_2, this prevents adsorption diffusion transport phenomena characterized by higher CO_2 permeances at lower temperatures observed for the BTESE membrane. The well-known formation of carbonates and/or carbamates on amine groups[30] could not be confirmed for our systems using XPS, as no shift of the N1s binding energy from 400 to 402 eV was detected. This means that the majority of the amine groups is present as in a non-protonated form. The increasing temperature dependence of the H_2/N_2 permeability ratio at higher PA concentrations could be typical for activated transport in microporous membranes.[31] However, similar pore sizes were measured by permporometry for all compositions. As a result, a decrease of the pore size cannot explain this observation. We propose that the increase of the content of PA in the network leads to a more flexible membrane structure. This flexibility then enhances the mobility of the network at higher temperatures and in turn leads to a faster H_2 permeation. The permeances of N_2 and CH_4 are less affected, as the pores are too small for these gases.

Turning to the pervaporation experiments, all membranes show reasonable to high fluxes in alcohol dehydration, despite their low gas permeances. Interestingly, the PA membranes have a higher selectivity in EtOH/water after testing in *n*-BuOH/H_2O. Possibly, this is related to the formation of multilayered adsorption of water, blocking larger pores for transport of the organic component (EtOH). Alternatively, butanol is irreversibly attached to the membrane. This would be consistent with the frequently found flux decrease over time in long term dehydration experiments.[10] An aging phenomenon by further polymerization of the silica structure[26] is unlikely to explain this behavior, as the water flux is not affected and only the solvent flux decreases strongly.

In gas permeation experiments, the permeabilities are linearly dependent on the concentration of the amino precursor. On the other hand, a minimum amine loading seems to be required in pervaporation to reach the optimal membrane performances. The permeate stream for all pervaporation experiments showed a high water concentration in the permeate for both *n*-BuOH and EtOH dehydration. The only exceptions were PA25 and IM25. The N/Si ratios of these membranes were 0.04 and 0.016 respectively, which correspond to an amino-functionalized precursors loading of respectively 6.4 and 1.6 mol%. In contrast, PA50 and IM50 membranes showed Si/N ratios corresponding to amino-functionalized precursor loading of 11.5 and 5.5 mol% respectively. A bimodal pore size distribution as already been observed for membranes based on mixtures of BTESE and triethoxysilanes.[9,32] It was ascribed to a limited interpenetration of the polymeric particles in the sol during drying. This could be a possible explanation for the poor performances of the PA25 and IM25. A minimum loading of the BTESE network between 6.4 and 11.5 mol% of PA precursor and between l.6 and 5.5 mol% of IM is required to counter the performance decrease from the assumed bimodal distribution of the PA25 and IM25. The LDA is apparently more easily accommodated in the BTESE network membranes and showed a minimum loading of 12.5 mol% and therefore exhibited constant high water purity in the permeate.

This minimum loading also indicates that there is no need to strive to a higher amine concentration in these microporous hybrid membranes. A low concentration of terminally

functionalized precursors enhances the network connectivity and this likely has a positive effect on the hydrothermal stability. XPS measurements show that a maximum loading of amino-functional groups in the BTESE matrix is reached, similar to Periodic Mesoporous Organosilicas (PMOs).[33,34] The observed low N/Si ratios cannot arise from thermal degradation during heat treatment or PA evaporation, as the values for both the dried and heat treated powders were equal to those expected. A more likely explanation is that the relatively short reaction time of the PA molecules promoted the formation of small clusters by hydrogen bonding[27] and that only a limited fraction of the PA molecules reacts with the BTESE oligomers present in the sol. The largest particles in the sol are deposited on the surface of the γ-alumina layer support layer, whereas the smaller sized fraction infiltrates into the γ-alumina layer. The depth profile obtained by XPS confirms this infiltration of an PA rich sol. Using the current procedures a maximum of 13.5% of PA and IM and 30–35% of LDA can be introduced in a BTESE network. Consequently, only small amounts of amino precursors are required to benefit from the hydrophilic properties of the amino-functionalized precursors.

Conclusions

We developed and characterized the first amino functionalized microporous hybrid silica membranes based on three precursors with different amine type, shape, and structure (PA, IM and LDA). After optimization of the sol synthesis, defect free membranes were obtained. Although the degree of incorporation was lower than expected, the highly polar nature of amine groups resulted in an increasing adsorption of water molecules in the pores with increasing concentration of amine functional group. As a consequence, the H_2 permeability decreased with an order of magnitude in the range from pure BTESE to pure PA membranes. Lower affinity for CO_2 due to shielding of adsorption sites by the adsorbed water molecules was also observed. Pervaporation measurements clearly showed that a minimum loading of amino-functionalized precursor is required to obtain water selective membranes. This minimum loading depends on the precursor and is between 6.4 and 11.5 mol% for PA and between 1.6 and 5.5 mol % for IM. After a first *n*-BuOH dehydration and independent of the precursor, all membranes with an effective amino loading higher than this threshold value proved to be highly efficient in dehydration of both EtOH and *n*-BuOH with respective permeate water purities of at least 90 and 95 wt%. All of these results clearly showed the ability to modify the affinity of BTESE-based membranes by introducing a suitable precursor. The result of this is a membrane type that is gas tight and at the same time highly water permeable. Further flux/selectivity optimization may be possible in the range of 10–20 mol% of amino-functionalized precursor. The unique properties of these amino-functionalized precursors allow for selectivity improvement which is not solely dependent on pore size or defect control, but also on affinity, and therefore open up a highly promising option.

Acknowledgements

The authors would like to acknowledge Gerard Kip from the MESA+ Nanolab of the University of Twente for the XPS measurements and the fruitful discussion on this subject.

Notes and references

1 C. Sanchez, B. Julian, P. Belleville and P. Popall, *J. Mater. Chem.*, 2005, **15**, 3559–3592.
2 R. M. de Vos and H. Verweij, *Science*, 1998, **279**, 1710–1711.
3 R. S. A. de Lange, J. H. A. Hekkink, K. Keizer and A. J. Burggraaf, *J. Membr. Sci.*, 1995, **99**(1), 57–75.
4 H. Imai, H. Morimoto, A. Tominaga and H. Hirashima, *J. Sol-Gel Sci. Technol.*, 1997, **10**, 45–54.
5 J. Campaniello, C. W. R. Engelen, W. G. Haije, P. P. A. C. Pex and J. F. Vente, *Chem. Commun.*, 2004, 834–835.
6 H. M. van Veen, Y. C. van Delft, C. W. R. Engelen and P. P. A. C. Pex, *Sep. Purif. Technol.*, 2001, **22–23**, 361–366.
7 H. L. Castricum, A. Sah, R. Kreiter, D. H. A. Blank, J. F. Vente and J. E. ten Elshof, *J. Mater. Chem.*, 2008, **18**, 2150–2158.
8 H. M. van Veen, M. D. Rietkerk, D. P. Shanahan, M. M. A. van Tuel, R. Kreiter, H. L. Castricum, J. E. ten Elshof and J. F. Vente, *J. Membr. Sci.*, 2011, **380**, 124–131.
9 R. Kreiter, M. D. A. Rietkerk, H. L. Castricum, H. M. van Veen, J. E. ten Elshof and J. F. Vente, *ChemSusChem*, 2009, **2**(2), 158–160.
10 M. Michau and M. Barboiu, *J. Mater. Chem.*, 2009, **19**, 6124–6131.
11 B. A. McCool and W. J. DeSisto, *Adv. Funct. Mater.*, 2008, **15**, 1635–1640.
12 H. L. Castricum, G. G. Paradis, M. C. Mittelmeijer-Hazeleger, R. Kreiter, J. F. Vente and J. E. ten Elshof, *Adv. Funct. Mater.*, 2011, **21**(9), 2319–2329.
13 N. Liu, R. A. Assink, B. Smarsly and C. J. Brinker, *Chem. Commun.*, 2003, 1146–1147.
14 G. S. Caravajal, D. E. Leyden, G. R. Quinting and G. E. Maciel, *Anal. Chem.*, 1988, **60**, 1776–1786.
15 N. Gartmann, C. Schütze, H. Ritter and D. Drühwiler, *J. Phys. Chem. Lett.*, 2010, **1**(1), 379–382.
16 J. C. Hicks, R. Dabestani, A. C. Buchanan and C. W. Jones, *Inorg. Chim. Acta*, 2008, **361**, 3024–3032.
17 I. A. Rahman, M. Jafarzadeh and C. S. Sipaut, *Ceram. Int.*, 2009, **35**, 1883–1888.
18 J. M. Rosenholm and M. Lindén, *Chem. Mater.*, 2007, **19**, 5023–5034.
19 M. Durrieu, S. Pallu, F. Guillemot, R. Bareille, J. Amédée and C. H. Baquey, *J. Mater. Sci.: Mater. Med.*, 2004, **15**, 779–786.
20 E. Verné, C. Vitale-Brovarone, E. Bui, C. L. Binachi and A. R. Boccaccini, *J. Biomed. Mater. Res., Part A*, 2009, **90A**, 981–992.
21 G. Xomeritakis, C. Y. Tsai and C. J. Brinker, *Sep. Purif. Technol.*, 2005, **42**(3), 249–257.
22 G. Xomeritakis, C. Y. Tsai, Y. B. Jiang and C. J. Brinker, *J. Membr. Sci.*, 2009, **341**(1–2), 30–36.
23 B. C. Bonekamp, A. J. Burggraaf and L. Cot, *Fundamentals of Inorganic Membrane Science and Technology*, Elsevier, Amsterdam, 1996, vol. 4.
24 F. T. Rusting, G. de Jong, P. P. A. C. Pex, and J. A. J. Peters, *Sealing Socket and Method for Arranging a Sealing Socket to a Tube*, *International Pat.*, WO 01/63162A1, 2001.
25 T. Tsuru, T. Hino, T. Yoshioka and M. Asaeda, *J. Membr. Sci.*, 2001, **186**(2), 257–265.
26 C. J. Brinker, and G. W. Scherer, *Sol–Gel Science—The Physics and Chemistry of Sol–Gel Processing*, Academic Press, New York, 1990.
27 J. C. Hicks, R. Dabestani, A. C. Buchanan and C. W. Jones, *Chem. Mater.*, 2006, **18**, 5022–5032.
28 R. S. A. de Lange, *Microporous Sol–Gel Derived Ceramic Membranes for Gas Separation*, Thesis dissertation, ISBN 90-9006558-X, University of Twente, 1993.
29 R. W. Baker, *Membrane Technology and Applications*, 2nd edn, 2007.
30 V. Zelenak, M. Badanicova, D. Halamova, J. Cejka, A. Zukal, N. Murafa and G. Goerigk, *Chem. Eng. J.*, 2008, **144**, 336–342.
31 R. S. A. de Lange, K. Keizer and A. J. Burggraaf, *J. Membr. Sci.*, 1995, **104**, 81–100.
32 C. J. Brinker, R. Sehgal, S. L. Hietala, R. Deshpande, D. M. Smith, D. A. Loy and C. S. Ashley, *J. Membr. Sci.*, 1994, **94**, 85–102.
33 M. C. Burleigh, M. A. Markowitz, M. S. Spector and B. P. Gaber, *Chem. Mater.*, 2001, **13**, 4760–4766.
34 M. C. Burleigh, M. A. Markowitz, M. S. Spector and B. P. Gaber, *J. Phys. Chem. B*, 2001, **105**, 9935–9942.

